Supplemental Material to "Radiative toroidal dipole and anapole excitations in collectively responding arrays of atoms"

K. E. Ballantine and J. Ruostekoski
Department of Physics, Lancaster University, Lancaster, LA1 4YB, United Kingdom
(Dated: July 28, 2020)

We include additional details of how the formalism employed in the main text for atomic transitions relates to effective oscillating currents and nanoresonator systems. We present a brief description of the mathematical model which applies both in the limit of low light intensity with coherent drive and to a single photon excitation in the absence of drive. We extend the discussion of the toroidal dipole eigenmode to the occupation of the mode. Additional details of how the proposal could be realized experimentally are considered. Finally we give results for simplified toroidal dipole and anapole unit cells with atoms only in a single 2D plane.

SI. LIGHT-ATOM INTERACTIONS

SI.A. Quantum system of atoms and light

In the main text we describe the excitation of an effective toroidal dipole and anapole in a coherently driven atomic ensemble by the equations $\dot{\mathbf{b}} = i\mathcal{H}\mathbf{b}+\mathbf{f}$ where $\mathbf{b}$ is a vector of atomic dipole amplitudes and $\mathbf{f}$ is proportional to the amplitude of the driving field. Here we describe the quantum model of atoms interacting with light in the *length gauge*, obtained by the Power-Zienau-Woolley transformation [S1–S4]. In the limit of low light intensity, the system with a single electronic ground state can be exactly described by a classical model of coupled dipoles driven by coherent light with field $\boldsymbol{\mathcal{E}}(\mathbf{r})$ [S5, S6]. The full many-excitation dynamics is described by the many-body quantum master equation for the density matrix [S7];

$$\begin{aligned}\dot{\rho} = i\sum_{j,\nu}[H_{j\nu},\rho] + i\sum_{jl\nu\mu(l\neq j)}\Omega^{(jl)}_{\nu\mu}\left[\hat{\sigma}^{+}_{j\nu}\hat{\sigma}^{-}_{l\mu},\rho\right] \\ + \sum_{jl\nu\mu}\gamma^{(jl)}_{\nu\mu}\left(2\hat{\sigma}^{-}_{l\mu}\rho\hat{\sigma}^{+}_{j\nu} - \hat{\sigma}^{+}_{j\nu}\hat{\sigma}^{-}_{l\mu}\rho - \rho\hat{\sigma}^{+}_{j\nu}\hat{\sigma}^{-}_{l\mu}\right),\end{aligned} \tag{S1}$$

with the square brackets representing commutators and

$$\begin{aligned}H_{j\nu} = \Delta^{(j)}_{\nu}\hat{\sigma}^{+}_{j\nu}\hat{\sigma}^{-}_{j\nu} \\ + \frac{\xi}{D}\hat{\mathbf{e}}_{\nu}\cdot\epsilon_0\mathcal{E}_0(\mathbf{r}_j)\hat{\sigma}^{+}_{j\nu} + \frac{\xi}{D}\hat{\mathbf{e}}^{*}_{\nu}\cdot\epsilon_0\mathcal{E}^{*}_0(\mathbf{r}_j)\hat{\sigma}^{-}_{j\nu},\end{aligned} \tag{S2}$$

where $\sigma^{+}_{j\nu} = |e\rangle_{j\nu j}\langle g|$ is the raising operator for atom j from its ground state to its excited state with $m=\nu$. Here, $\Delta^{(j)}_{\nu}$ is the detuning of each level from resonance. The Hermitian interaction terms $\Omega^{(jl)}_{\nu\mu}$ and collective dissipation terms $\gamma^{(jl)}_{\nu\mu}$ due to the dipole-dipole coupling between the atoms are given by the real and imaginary part of

$$\Omega^{(jl)}_{\nu\mu} + i\gamma^{(jl)}_{\nu\mu} = \xi\mathcal{G}^{(jl)}_{\nu\mu}, \tag{S3}$$

where $\mathcal{G}^{(jk)}_{\nu\mu} = \hat{\mathbf{e}}_{\nu}\cdot\mathsf{G}(\mathbf{r}_i-\mathbf{r}_j)\hat{\mathbf{e}}_{\mu}$ is the dipole radiation kernel that, acting on a dipole $\mathbf{d}$ at the origin, produces the familiar expression [S8] (with $\hat{\mathbf{r}} = \mathbf{r}/|\mathbf{r}|$)

$$\begin{aligned}\mathsf{G}(\mathbf{r})\mathbf{d} = -\frac{\mathbf{d}\delta(\mathbf{r})}{3} + \frac{k^3}{4\pi}\Bigg\{(\hat{\mathbf{r}}\times\mathbf{d})\times\hat{\mathbf{r}}\frac{e^{ikr}}{kr} \\ - \left[3\hat{\mathbf{r}}\left(\hat{\mathbf{r}}\cdot\mathbf{d}\right) - \mathbf{d}\right]\left[\frac{i}{(kr)^2} - \frac{1}{(kr)^3}\right]e^{ikr}\Bigg\},\end{aligned} \tag{S4}$$

and $\xi = 6\pi\gamma/k^3$.

SI.B. Low light intensity limit

In the limit of low drive intensity we neglect terms containing products of two or more excited state amplitudes, or one or more excited state amplitudes multiplied by the drive field [S4]. In our system, this amounts to neglecting terms $\langle\sigma^{+}_{j\nu}\sigma^{-}_{\ell\mu}\rangle$ (along with higher order correlators of $\sigma^{\pm}_{j\nu}$) and $\mathcal{E}_0\langle\sigma^{+}_{m}\rangle$. The excited state population is negligible while the ground state population is invariant. The only non-trivial equation is for $\langle\sigma^{-}_{j\nu}\rangle$ and Eq. S1 reduces to

$$\dot{\mathbf{b}} = i\mathcal{H}\mathbf{b} + \mathbf{f}, \tag{S5}$$

in terms of the vector $b_{3j+\nu-1} = \langle\sigma^{-}_{j\nu}\rangle$, the matrix

$$\mathcal{H}_{3j+\nu-1,3k+\mu-1} = \Delta^{(j)}_{\nu}\delta_{\nu\mu}\delta_{jk} + \Omega^{(jk)}_{\nu\mu}(1-\delta_{jk}) + i\gamma^{(jk)}_{\nu\mu}, \tag{S6}$$

and the drive $f_{3j+\nu-1} = i(\xi/\mathcal{D})\hat{\mathbf{e}}_{\nu}\cdot\epsilon\boldsymbol{\mathcal{E}}(\mathbf{r}_j)$.

SI.C. Single photon excitation

The dynamics of a single photon excitation, decaying in the absence of drive, can also be described by the same formalism. Without drive, there is decay from the single-excitation state to the ground state, but the remaining single-excitation state remains pure, and the dynamics

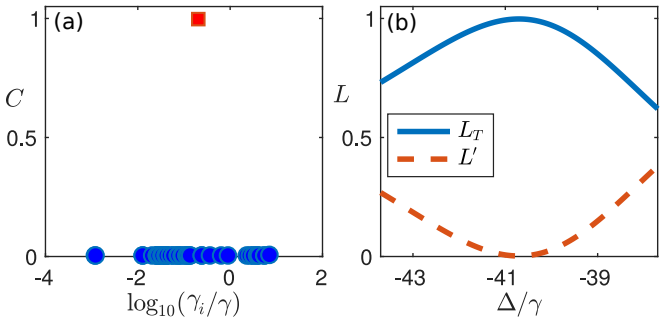

FIG. S1. (a) Overlap of each eigenmode of a toroidal dipole unit cell (ordered by the collective resonance linewidth) with an ideal toroidal dipole mode with poloidal polarization. (b) Occupation measure L_T of the toroidal dipole collective eigenmode and sum L' of the occupation of all other modes in the steady state response, as laser detuning is varied, for $r = 0.2\lambda$, $a = 0.08\lambda$.

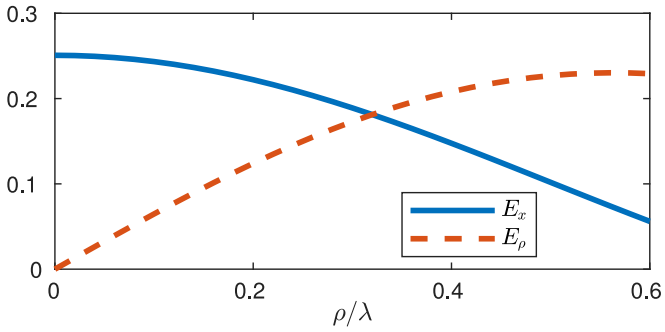

FIG. S2. Longitudinal component $|E_x|$ and radial component $|E_\rho|$ of the focused radially polarized beam used to excite the anapole, as a function of the distance $\rho = \sqrt{y^2 + z^2}$ from the beam axis in the focal plane $x = 0$. Here the incoming field before focusing is $\boldsymbol{\mathcal{E}} = \hat{\mathbf{e}}_\rho$ and the NA is 0.7.

is linear in the amplitude of this state. It is this linear response without saturation which provides identical single-particle amplitudes to those of the low light intensity limit of coherently driven atoms [S9].

We again start from the full atomic equations of motion Eq. S1, but now assume that the initial state consists of a pure, single-photon excitation. Then the density matrix at later times can be written as

$$\rho = |\Psi\rangle\langle\Psi| + p_g |G\rangle\langle G|, \tag{S7}$$

where $|\Psi\rangle$ is a state consisting of exactly one excitation, $|G\rangle$ is the state with all atoms in their ground state, and p_g is the probability that the excitation has decayed. In this case there is no incoherent mixing between the excited and ground state. While dissipation means that the norm of $|\Psi\rangle$ is not conserved, the dynamics within the single-excitation subspace is coherent, and it can always be expanded in terms of the individual atomic excitations

$$|\Psi\rangle = \sum_{j,\nu} \mathcal{P}_\nu^{(j)}(t)\, \hat{\sigma}_{j\nu}^{+} |G\rangle, \tag{S8}$$

with amplitudes $\mathcal{P}_\nu^{(j)}(t)$. For single-particle expectation values, the dynamics can equally be written in terms of these amplitudes. In terms of the vector $b_{3j+\nu-1} = \mathcal{P}_\nu^{(j)}$, we have again $\dot{\mathbf{b}} = i\mathcal{H}\mathbf{b}$ [S10], formally equivalent to the equations describing the low light intensity limit in the absence of drive. The identical description is due to the fact that in each case the relevant dynamics includes only a part of the density matrix which evolves linearly without saturation, with the collective response being determined by the dipole propagation kernel $\mathcal{G}_{\nu\mu}^{(jl)}$.

SII. COLLECTIVE TOROIDAL EIGENMODE

The collective dynamics of the atomic ensemble is determined by the eigenvectors $\mathbf{v}_j$ of $\mathcal{H}$, representing the collective radiative excitation eigenmodes of the atoms, and the corresponding eigenvalues $\delta_j + i\gamma_j$ [S11], where γ_j denotes the collective resonance linewidth and δ_j the collective resonance line shift from the single-atom resonance. While these eigenvectors are not orthogonal in general, they do form a basis, and the state can be expanded at all times as $\mathbf{b}(t) = \sum_i c_i(t)\mathbf{v}_i$. The occupation of each eigenmode can then be defined as [S12]

$$L_i = \frac{|\mathbf{v}_i^T \mathbf{b}|^2}{\sum_j |\mathbf{v}_j^T \mathbf{b}|^2}. \tag{S9}$$

For a single-photon excitation, each eigenmode will decay individually with

$$c_j(t) = \exp\left[(i\delta_j - \gamma_j)t\right], \tag{S10}$$

with $c_j(0)$ determined by the initial state.

The toroidal dipole unit cell has a collective eigenmode exhibiting a strong toroidal dipole as discussed in the main text. We can similarly measure the overlap of this mode with an ideal toroidal dipole eigenmode $\mathbf{v}_T$, depicted in Fig. 1 of the main text, with poloidal polarization. This is given by $C_i = |\mathbf{v}_i^T \mathbf{v}_T|^2 / \sum_j |\mathbf{v}_j^T \mathbf{v}_T|^2$. This overlap is illustrated for each eigenmode in Fig. S1(a) showing that there is a unique collective mode which approximates the ideal poloidal polarization mode. The occupation L_T of this eigenmode, as well as the sum of occupations of all other modes, is plotted in Fig. S1(b) as a function of laser detuning, with $L_T > 0.99$ at resonance. The maximum occupation in Fig. S1 corresponds to the maximum toroidal dipole excitation of Fig. 3 in the main text.

SIII. CLASSICAL ANALOGUE OF POLARIZATION DISTRIBUTION

In this work, we have synthesized collective radiative excitations of atoms that produce a toroidal dipole and an anapole. This is achieved by a simple arrangement of

atoms that experience strong light-mediated interactions. In particular, the toroidal dipole is generated by the orientation of the atomic transitions due to the dipole-dipole interactions forming an effective poloidal electric current wound around a torus. Each atom produces an effective electric dipole generated by quantum-mechanical electric-dipole-allowed transitions in electronic orbitals. Here we provide a classical analogue description of this quantum-mechanical process, illustrating how effective polarization and current densities originate from such atomic dipole transitions. This allows us to make comparisons with systems of nanoparticles and solid-state artificial metamaterial resonators that have been used in studies of electromagnetic multipole radiation.

SIII.A. Classical effective currents from trapped atoms

Classically, we describe the interactions of light with atoms trapped in a ring-shaped pattern, represented by a sequence of oscillating charges. Consider a ring in the xy plane with radius ρ, and let ϕ be the azimuthal angle in the plane. Suppose there is a flow of charge on the ring and consider an infinitesimal segment where a negative charge $-q$ moves from a point $\mathbf{r}_\phi$ at angle ϕ a distance $\Delta\mathbf{r} = -\rho\,\mathrm{d}\phi\hat{\phi}$ along the ring in a time $\mathrm{d}t$, leaving a positive charge q stationary at $\mathbf{r}_\phi$. The charge distribution can be replaced by n dipoles with spacing $\Delta r/n$ such that the positive charge of each dipole overlaps with the negative charge of the next, leaving only the original charges at each end. Then the polarization density in the limit $n \to \infty$ is [S3]

$$\begin{aligned}\mathbf{P} = \lim_{n\to\infty}\sum_{p=0}^{n-1}(-q)\,\frac{\Delta\mathbf{r}}{n}\delta\left(\mathbf{r} - \left(\mathbf{r}_\phi + \frac{p+1/2}{n}\right)\Delta\mathbf{r}\right) \\ = -\int_0^1 \mathrm{d}u\, q\Delta\mathbf{r}\delta(\mathbf{r} - \mathbf{r}_\phi - u\Delta\mathbf{r}),\end{aligned} \tag{S11}$$

giving a continuous polarization density consisting of point dipoles $\mathrm{d}\mathbf{P} = -q\Delta\mathbf{r}\delta(\mathbf{r}-\mathbf{r}_\phi-u\Delta\mathbf{r})\mathrm{d}u = q\rho\,\mathrm{d}\phi\,\delta(\mathbf{r}-\mathbf{r}_\phi - u\Delta\mathbf{r})\mathrm{d}u\hat{\phi}$ located at $\mathbf{r}_\phi + u\Delta\mathbf{r}$ and pointing in the direction $\hat{\phi}$. These point dipoles describe the response of single atoms, whose size is negligible compared to the optical wavelength.

The current density associated with the change in the electric charge distribution from each point dipole is given by

$$\begin{aligned}\mathrm{d}\mathbf{J} &= \frac{1}{\mathrm{d}t}[-q(\mathbf{r}_\phi + \Delta\mathbf{r}_\phi) - (-q)\mathbf{r}_\phi]\delta(\mathbf{r} - \mathbf{r}_\phi - u\Delta\mathbf{r})\mathrm{d}u, \\ &= q\rho\frac{\mathrm{d}\phi}{\mathrm{d}t}\delta(\mathbf{r} - \mathbf{r}_\phi - u\Delta\mathbf{r})\mathrm{d}u\hat{\phi},\end{aligned} \tag{S12}$$

which is simply equal to $\mathrm{d}\mathbf{P}/\mathrm{d}t$. This circulating current, for a sufficiently small circle, creates an effective magnetic dipole with a magnetic moment $d\mu = \mathrm{d}u(q/(2\mathrm{d}t))\mathbf{r}_\phi \times \Delta\mathbf{r} = \mathrm{d}u(q\rho^2\mathrm{d}\phi/(2\mathrm{d}t))\hat{\mathbf{z}}$ such that the total magnetic moment $\mu = \int \mathrm{d}\mu = (\mathrm{d}\phi\rho^2/2)(q/\mathrm{d}t)\hat{\mathbf{z}}$ is simply the current times the area of the circle within the angle $\mathrm{d}\phi$.

While this description applies to a continuous distribution of dipoles located at $\mathbf{r}_\phi + u\Delta\mathbf{r}$ (or n discreet dipoles without taking the limit $n \to \infty$ in Eq. S11), it can be approximated with a discrete series of a smaller number of dipoles located at fixed positions $\mathbf{r}_j$. The corresponding polarization density $P_\sigma(\mathbf{r},t) = \exp(-i\omega t)\mathcal{D}\sum_j \mathcal{P}_\sigma^{(j)}\delta(\mathbf{r}-\mathbf{r}_j)$ induced by a driving field with frequency ω leads to a current density $\mathbf{J} = -i\omega\mathbf{P}$. When these discrete currents are arranged to point tangentially to a circle, they approximate a closed loop of current. The magnetic dipole moment appearing in the scattering cross section is then [S13] $\mathbf{m} = \mu/c = 1/(2c)\int \mathrm{d}^3\mathbf{r}\,\mathbf{r}\times\mathbf{J}(\mathbf{r})$. Similarly, poloidal current distributions are approximated by currents from time dependent point dipoles giving a toroidal dipole moment [S14]

$$\mathbf{T} = \frac{1}{10c}\int \mathrm{d}^3\mathbf{r}\left[\mathbf{r}(\mathbf{r}\cdot\mathbf{J}) - 2\mathbf{r}^2\mathbf{J}\right]. \tag{S13}$$

Numerically, we include all the light-mediated dipole-dipole interactions between the atoms and calculate the collective excitation eigenmodes for the coupled dipoles (see Sec. SII). One of the eigenmodes then corresponds to the poloidal current configuration of the toroidal dipole [Fig. S1(a)]. This also applies to the case of an array of several toroidal dipoles, as discussed in the main text.

SIII.B. Nanoparticles and solid-state resonators

The classical description of the effective current due to atomic dipole transitions, given in the previous section, allows us to make comparisons with systems of nanoparticles and resonators in artificial metamaterials that form multipole radiation sources. The most dramatic difference is the quantum-mechanical nature of the optical interaction for the case of atoms, where the atomic transitions are determined by the precise resonance frequency and the quantum-mechanical Wigner-Weisskopf resonance linewidth [S3]. Atoms also form truly point-like electric dipoles.

In the limit of low light intensity, the atoms interacting with incident light can be considered as a linear classical coupled-dipole system (see Sec. SI SI.B). Small nanoparticles [S15, S16] or circuit resonators [S17, S18] are frequently approximated as effective coupled point dipoles in electromagnetic fields. Nanoparticles with their electric dipoles (provided that the higher-order multipole contributions are negligible) forming a closed ring can then exhibit a mode that behaves as an effective magnetic dipole [S15], analogously to the earlier classical charge distribution description of the atoms. In resonant LCR circuits in metamaterials, the current oscillations form effective electric and magnetic dipoles that radiatively

couple with the current oscillations of the other circuits. If each circuit is modeled as a pointlike particle, and higher-order multipole contributions of each circuit are negligible, the dynamics corresponds to a coupled-dipole system [S17, S18].

As a comparative example, a nanorod can be approximated as an effective point dipole [S19], where the polarization density is to first order assumed to be a uniform distribution of point dipoles throughout the volume of the rod. Depending on the geometry of the problem and the thickness of the nanorods, all other excitation modes, such as radial or azimuthal currents are then in this approximation ignored. For a single nanorod of radius a and length H at the origin, and aligned along the z axis, the resulting polarization distribution is

$$\mathbf{P} = \frac{\mathcal{Q}(t)}{\pi a^2}\hat{\mathbf{z}}\Theta(a-\rho)\Theta(H/2-z)\Theta(H/2+z), \qquad \text{(S14)}$$

where Θ is the Heaviside function, $\rho = \sqrt{x^2+y^2}$, and $\mathcal{Q}(t)$ is a generalized coordinate whose derivative $\dot{\mathcal{Q}}(t)$ describes current oscillations in the nanorod. In contrast to atomic dipoles, although for $H \lesssim \lambda$ this polarization density can be approximated by a point dipole $\mathbf{P} = \mathcal{Q}(t)H\hat{\mathbf{z}}\delta(\mathbf{r})$, this approximation easily breaks down for interacting nanorods that are too closely separated compared with the resonant wavelength [S19].

SIV. EXPERIMENTAL CONSIDERATIONS

For most of the examples discussed in the main text we choose $r = (n+1/2)a$ for integer n, with the result that the atoms lie on selected sites of a square lattice with lattice constant a (see main text Fig. 2). Four intersecting beams, two pairs of propagating beams in the y and z directions respectively, can be used to produce such a lattice with confining potential

$$V(\mathbf{r}) = sE_R\left[\sin^2\left(\pi\frac{y}{a}\right) + \sin^2\left(\pi\frac{z}{a}\right)\right], \qquad \text{(S15)}$$

where $E_R = \pi^2\hbar^2/(2ma^2)$ is the lattice recoil energy and s is a dimensionless constant which determines the depth of the lattice [S20]. An additional potential can confine the atoms in the $x = \pm a/2$ planes. This could be an identical pair of counter-propagating beams in the x direction, or a simpler double-well potential. Locally, each atom experiences a harmonic trapping potential $V(\mathbf{r}) = (m/2)\sum\omega_\mu^2(\Delta r_\mu)^2$ where $\omega_{y,z} = 2\sqrt{s}E_R/\hbar$, ω_x is the harmonic trapping frequency in the x direction, and $\Delta\mathbf{r}$ is the displacement from the center of the lattice site. Then the atom at site $\mathbf{r}_j$ has a Wannier function $\phi_j(\mathbf{r}) = \phi(\mathbf{r}-\mathbf{r}_j)$ given by

$$\phi(\mathbf{r}) = \frac{1}{(\pi^3 l^4 l_x^2)^{1/4}}\exp\left(-\frac{y^2+z^2}{2l^2} - \frac{x^2}{2l_x^2}\right), \qquad \text{(S16)}$$

with width $l = as^{-1/4}/\pi$ and thickness $l_x = \sqrt{\hbar/(m\omega_x)}$. The atoms can be increasingly strongly confined by increasing the trapping strength s. Experimentally, atoms are loaded deterministically into a Mott-insulator state with one atom per site [S21–S23], and the desired geometry achieved by removing excess atoms on a site-by-site basis [S24].

Further techniques have also been developed to provide deeply subwavelength features in optical trapping potentials. For example, coupling three atoms in a Λ configuration via a strong control field with Rabi frequency $\Omega_c(y,z) = \Omega_c\sin(ky)\sin(kz)$ and a weak probe field with Rabi frequency Ω_p leads to a trapping potential which depends on the ratio $\Omega_c(y,z)/\Omega_p$, which varies rapidly in a small region close to the nodes of $\Omega_c(y,z)$, for $\Omega_p/\Omega_c \ll 1$ [S25]. Alternatively, internal degrees of freedom can be exploited [S26]. Lattices with periodicity less than half the wavelength of the control field can also be engineered by stroboscopicaly shifting the lattice at high frequency such that the atoms experience a time-averaged potential with higher periodicity than the instantaneous potential at any one time [S27, S28]. Finally, optical tweezers provide an alternative means to design arbitrary potentials [S29–S31] with single-site control [S32, S33].

Atoms such as Sr and Yb are particularly suitable for subwavelength trapping. ^{33}Sr has a transition between the $^3P_0$ state and the triply degenerate $^3D_1$ state [S34] with wavelength $\lambda = 2.6\mu$m and linewidth $\Gamma = 2.9\times 10^5$/s. The magic wavelength for these states gives an optical lattice with spacing $d = 206.4$nm, less than $\lambda/10$. While most of the examples we consider require varying only the overall laser detuning, the data shown in Fig. 4 of the main text requires the individual atomic level shifts of different atoms to be controlled. This could be achieved by ac Stark shifts [S35] from standing wave lasers offset from the trapping lattice such that different sites experience different intensities.

SV. ANAPOLE EXCITATION

To excite the anapole we use a tightly focused radially polarized beam. The focusing leads to a longitudinal component in the x direction on the beam axis which directly drives the x component of polarization on the two atoms at the center of the anapole. Off axis, a combination of radial and longitudinal polarization couple to the toroidal dipole mode of the remaining atoms. The amplitude of the longitudinal and radial components of the field in the $x = 0$ focal plane are shown in Fig. S2 as a function of the radial distance ρ from the beam axis.

SVI. IN-PLANE TOROIDAL DIPOLE AND ANAPOLE

An experimentally even simpler realization of both the toroidal dipole and the anapole with atoms confined only to a single plane can be achieved by removing the atoms for which $z \neq 0$, as shown in Fig. 2(c) of the main

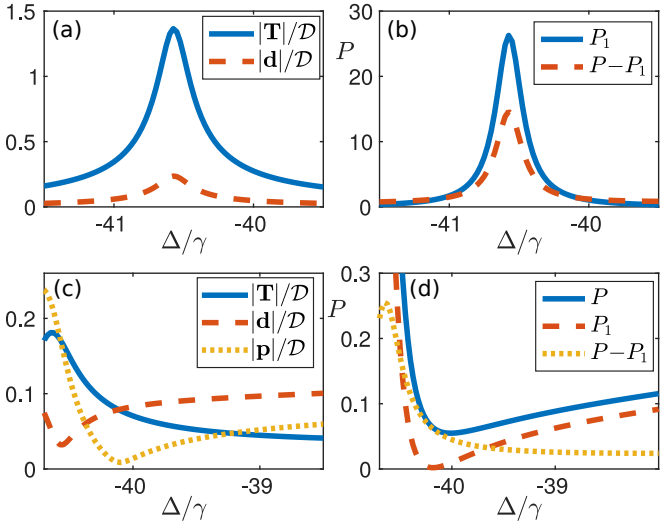

FIG. S3. Excitation of toroidal dipole and dynamic anapole with two magnetic dipole moments such that all atoms are in the single xy plane. Multipole decomposition for toroidal dipole unit cell of (a) atomic dipoles [in units of $\mathcal{D}\mathcal{E}_0/(\hbar\gamma)$], and (b) the far-field scattered light, separated into the total dipole component, and the remaining sum of all other contributions (in units of incident light intensity $I_{\rm in}/k^2$). Multipole decomposition for the single-plane dynamic anapole of (c) atomic dipoles [in units of $\mathcal{D}\mathcal{E}_0/(\hbar\gamma)$], with $\mathbf{p} = \mathbf{d} + ik\mathbf{T}$, and (d) the far-field scattered light, separated into the total dipole component, and the remaining sum all other contributions (in units of $I_{\rm in}/k^2$). In all cases $r = 0.2\lambda$ and $a = 0.08\lambda$.

text, leaving two squares with opposite chirality polarization. These squares will have magnetic dipole moments pointing in the $\hat{\mathbf{z}}$ and $-\hat{\mathbf{z}}$ directions, respectively, leading to zero net magnetic moment but contributing to a toroidal dipole. The resulting multipole decomposition of the atomic dipoles and the far-field scattered light is shown in Fig. S3(a,b). A strong toroidal dipole is present, although the far-field scattered light in this case also shows a comparable contribution from higher order modes. Again this toroidal dipole can interfere with a net electric dipole moment on two atoms at $\pm(a/2)\hat{\mathbf{x}}$ to form an anapole. The resulting multipole decomposition is shown in Fig. S3(c,d). There is strong suppression of the total dipole moment and a significant dip in the scattered light, although again the contributions of other multipole moments, especially quadrupoles, is stronger than the case with four squares presented in the main text. These contributions of higher-order multipole moments could be further suppressed by adding more atomic squares, 8, 16, etc.

[S1] E. A. Power and S. Zienau, "Coulomb gauge in non-relativistic quantum electro-dynamics and the shape of spectral lines," Philos. Trans. R. Soc. **251**, 427 (1959).

[S2] R. G. Woolley, "Molecular quantum electrodynamics," Proc. R. Soc. Lond. A **321**, 557–572 (1971).

[S3] Claude Cohen-Tannaudji, Jacques Dupont-Roc, and Gilbert Grynberg, *Photons and Atoms: Introduction to Quantum Electrodynamics* (John Wiley & Sons, New York, 1989).

[S4] Janne Ruostekoski and Juha Javanainen, "Quantum field theory of cooperative atom response: Low light intensity," Phys. Rev. A **55**, 513–526 (1997).

[S5] Juha Javanainen, Janne Ruostekoski, Bjarne Vestergaard, and Matthew R. Francis, "One-dimensional modeling of light propagation in dense and degenerate samples," Phys. Rev. A **59**, 649–666 (1999).

[S6] Mark D. Lee, Stewart D. Jenkins, and Janne Ruostekoski, "Stochastic methods for light propagation and recurrent scattering in saturated and nonsaturated atomic ensembles," Phys. Rev. A **93**, 063803 (2016).

[S7] R. H. Lehmberg, "Radiation from an n-atom system. i. general formalism," Phys. Rev. A **2**, 883–888 (1970).

[S8] John David Jackson, *Classical Electrodynamics*, 3rd ed. (Wiley, New York, 1999).

[S9] Anatoly A. Svidzinsky, Jun-Tao Chang, and Marlan O. Scully, "Cooperative spontaneous emission of n atoms: Many-body eigenstates, the effect of virtual Lamb shift processes, and analogy with radiation of n classical oscillators," Phys. Rev. A **81**, 053821 (2010).

[S10] K. E. Ballantine and J. Ruostekoski, "Subradiance-protected excitation spreading in the generation of collimated photon emission from an atomic array," Phys. Rev. Research **2**, 023086 (2020).

[S11] S. D. Jenkins, J. Ruostekoski, J. Javanainen, S. Jennewein, R. Bourgain, J. Pellegrino, Y. R. P. Sortais, and A. Browaeys, "Collective resonance fluorescence in small and dense atom clouds: Comparison between theory and experiment," Phys. Rev. A **94**, 023842 (2016).

[S12] G. Facchinetti, S. D. Jenkins, and J. Ruostekoski, "Storing light with subradiant correlations in arrays of atoms," Phys. Rev. Lett. **117**, 243601 (2016).

[S13] Rasoul Alaee, Carsten Rockstuhl, and I. Fernandez-Corbaton, "An electromagnetic multipole expansion beyond the long-wavelength approximation," Optics Communications **407**, 17 – 21 (2018).

[S14] N. Papasimakis, V. A. Fedotov, V. Savinov, T. A. Raybould, and N. I. Zheludev, "Electromagnetic toroidal excitations in matter and free space," Nat. Mater. **15**, 263–271 (2016).

[S15] Andrea Alù and Nader Engheta, "Dynamical theory of artificial optical magnetism produced by rings of plasmonic nanoparticles," Phys. Rev. B **78**, 085112 (2008).

[S16] Andrey B. Evlyukhin, Carsten Reinhardt, Andreas Seidel, Boris S. Luk'yanchuk, and Boris N. Chichkov, "Optical response features of si-nanoparticle arrays," Phys. Rev. B **82**, 045404 (2010).

[S17] S. D. Jenkins and J. Ruostekoski, "Theoretical formalism for collective electromagnetic response of discrete metamaterial systems," Phys. Rev. B **86**, 085116 (2012).

[S18] Stewart D. Jenkins and Janne Ruostekoski, "Metamaterial transparency induced by cooperative electromagnetic interactions," Phys. Rev. Lett. **111**, 147401 (2013).

[S19] Derek W. Watson, Stewart D. Jenkins, Vassili A. Fedotov, and Janne Ruostekoski, "Point-dipole approximation for small systems of strongly coupled radiating nanorods," Scientific Reports **9**, 5707 (2019).

[S20] Oliver Morsch and Markus Oberthaler, "Dynamics of bose-einstein condensates in optical lattices," Rev. Mod. Phys. **78**, 179–215 (2006).

[S21] U. Schnorrberger, J. D. Thompson, S. Trotzky, R. Pugatch, N. Davidson, S. Kuhr, and I. Bloch, "Electromagnetically induced transparency and light storage in an atomic mott insulator," Phys. Rev. Lett. **103**, 033003 (2009).

[S22] Jacob F. Sherson, Christof Weitenberg, Manuel Endres, Marc Cheneau, Immanuel Bloch, and Stefan Kuhr, "Single-atom-resolved fluorescence imaging of an atomic mott insulator," Nature **467**, 68–72 (2010).

[S23] Jun Rui, David Wei, Antonio Rubio-Abadal, Simon Hollerith, Johannes Zeiher, Dan M. Stamper-Kurn, Christian Gross, and Immanuel Bloch, "A subradiant optical mirror formed by a single structured atomic layer," (2020), arXiv:2001.00795 [quant-ph].

[S24] Christof Weitenberg, Manuel Endres, Jacob F. Sherson, Marc Cheneau, Peter Schauß, Takeshi Fukuhara, Immanuel Bloch, and Stefan Kuhr, "Single-spin addressing in an atomic mott insulator," Nature **471**, 319–324 (2011).

[S25] Y. Wang, S. Subhankar, P. Bienias, M. Łkacki, T-C. Tsui, M. A. Baranov, A. V. Gorshkov, P. Zoller, J. V. Porto, and S. L. Rolston, "Dark state optical lattice with a subwavelength spatial structure," Phys. Rev. Lett. **120**, 083601 (2018).

[S26] R. P. Anderson, D. Trypogeorgos, A. Valdés-Curiel, Q.-Y. Liang, J. Tao, M. Zhao, T. Andrijauskas, G. Juzeliūnas, and I. B. Spielman, "Realization of a deeply subwavelength adiabatic optical lattice," Phys. Rev. Research **2**, 013149 (2020).

[S27] Sylvain Nascimbene, Nathan Goldman, Nigel R. Cooper, and Jean Dalibard, "Dynamic optical lattices of subwavelength spacing for ultracold atoms," Phys. Rev. Lett. **115**, 140401 (2015).

[S28] M. Lacki, P. Zoller, and M. A. Baranov, "Stroboscopic painting of optical potentials for atoms with subwavelength resolution," Phys. Rev. A **100**, 033610 (2019).

[S29] T. Xia, M. Lichtman, K. Maller, A. W. Carr, M. J. Piotrowicz, L. Isenhower, and M. Saffman, "Randomized benchmarking of single-qubit gates in a 2d array of neutral-atom qubits," Phys. Rev. Lett. **114**, 100503 (2015).

[S30] Brian J. Lester, Niclas Luick, Adam M. Kaufman, Collin M. Reynolds, and Cindy A. Regal, "Rapid production of uniformly filled arrays of neutral atoms," Phys. Rev. Lett. **115**, 073003 (2015).

[S31] Alexandre Cooper, Jacob P. Covey, Ivaylo S. Madjarov, Sergey G. Porsev, Marianna S. Safronova, and Manuel Endres, "Alkaline-earth atoms in optical tweezers," Phys. Rev. X **8**, 041055 (2018).

[S32] Manuel Endres, Hannes Bernien, Alexander Keesling, Harry Levine, Eric R. Anschuetz, Alexandre Krajenbrink, Crystal Senko, Vladan Vuletic, Markus Greiner, and Mikhail D. Lukin, "Atom-by-atom assembly of defect-free one-dimensional cold atom arrays," Science **354**, 1024–1027 (2016).

[S33] Daniel Barredo, Sylvain de Léséleuc, Vincent Lienhard, Thierry Lahaye, and Antoine Browaeys, "An atom-by-atom assembler of defect-free arbitrary two-dimensional atomic arrays," Science **354**, 1021–1023 (2016).

[S34] B. Olmos, D. Yu, Y. Singh, F. Schreck, K. Bongs, and I. Lesanovsky, "Long-range interacting many-body systems with alkaline-earth-metal atoms," Phys. Rev. Lett. **110**, 143602 (2013).

[S35] Fabrice Gerbier, Artur Widera, Simon Fölling, Olaf Mandel, and Immanuel Bloch, "Resonant control of spin dynamics in ultracold quantum gases by microwave dressing," Phys. Rev. A **73**, 041602 (2006).